Atmospheric variations in summertime column integrated CO_2 on synoptic and seasonal time scale over the U.S.

Qingyu. Wang[1], Sean. M. R. Crowell[1] , Sandip Pal[2]

1School of Meteorology, University of Oklahoma, Norman, Oklahoma, USA

2 Department of Geosciences, Texas Tech University, Lubbock, Texas, USA

Corresponding author: Qingyu Wang (Qingyu.Wang-1@ou.edu)

Key Points:

- XCO_2 frontal differences over the US are positive in summer.
- Significance test show XCO_2 frontal differences are greater than when there is no front.

Abstract

Past studies have demonstrated that synoptic weather events play an important role in the spatial and temporal variations of atmospheric carbon dioxide (CO_2) within and above the boundary layer. In this study, we investigate the spatial variability of column average CO2 dry air mole fraction (XCO_2) due to the impact of synoptic scale transport using retrievals from the Orbiting Carbon Observatory-2 for 66 summer cold frontal cases over the conterminous U.S. and Mexico above 20°N from 2015 to 2019. The results show that these 66 XCO_2 differences across cold fronts in summer are in general agreement with data from the Atmospheric Chemistry and Transport (ACT-America) field campaign observations, which are significantly different compared to non-frontal XCO_2 spatial distributions in summer, though with reduced magnitude due to their nature as a column average as opposed to an *in situ* measurements in the boundary layer and free troposphere.

1 Introduction

The 30-year period from 1983 to 2012 has been reported to be the warmest period in the past 800 years [*Pachauri et al.*, 2014]. Also, sea level rise explained by about 75% by glacier mass loss and ocean thermal expansion, and CO_2 concentrations increased at the fastest observed decadal rate of change for 2002-2011 by IPCC Fifth Assessment Report [*Pachauri et al.*, 2014] . The increase of the amount of greenhouse gases (GHGs) and unbalanced carbon cycle drive global climate warming (Reference et al.?). Observations of CO_2 dry air mole fraction are critical for constraining estimates of surface fluxes at global and regional scales. CO_2 is measured *in situ* in the atmospheric boundary layer by the Global Greenhouse Gas Reference Network [*Gurney et al.*, 2002; 2003; *Law et al.*, 2006; *Masarie et al.*, 2014; *Masarie et al.*, 2001], which is coordinated by the Global Monitoring Division (GMD) in the Earth System Research Laboratory (ESRL) at the National Oceanic and Atmospheric Administration (NOAA). Light aircraft samples are returned on an approximately biweekly cadence at many of these sites as well. The Total Carbon Column Observing Network (TCCON, https://tccon-wiki.caltech.edu/Sites) retrieves XCO_2 with a similar density of observations globally. Field campaigns such as the HIAPER Pole to Pole Observations (HIPPO, *Wofsy* [2011]) study, the Atmospheric Tomography (ATom) experiments (https://daac.ornl.gov/ATOM/campaign/), and the O2/N2 Ratio and CO_2 Airborne Southern Ocean (ORCAS) Study [*Stephens et al.*, 2017] have targeted larger scale variations in CO_2 with *in situ* measurements of CO_2 mole fractions as well as other tracers. Currently, the Atmospheric Chemistry and Transport (ACT)-America experiment targets synoptic scale variations in CO_2 with both *in situ* measurements and CO_2 lidar observations in North America (Bell et al., 2020; Campbell et al., 2020). Remote sensing retrievals from satellites such as the Orbiting Carbon Observatory-2 (OCO-2) provide global coverage using reflected sunlight to infer XCO_2. Regardless of the source, the overall goal of data collection is to better understand the carbon cycle with a “top-down” constraint of surface fluxes of CO_2.

Atmospheric CO_2 variability is directly affected by the combined impact of surface fluxes and atmospheric transport [*Enting*, 2002]. Thus, inferring surface fluxes from observations requires an understanding of the fingerprint of transport effects on the data in question (Schuh et al, 2018). In this paper, we examine the signature of frontal boundaries on XCO_2 spatial

distribution at warm and cold sectors in OCO-2 retrievals and evaluate their structure against previous studies using surface data as well as current observations made during the ACT-America field campaign.

2 Background

Fronts are often initiated by large-scale horizontal deformation field — the tendency of air parcels to change shape, and result in sharp temperature contrasts and precipitation [*Wallace and Hobbs*, 2006]. *Hurwitz et al.* [2004] demonstrated that abrupt changes in CO_2 mixing ratio happened in the presence of inclement weather and low pressure systems as detected through observations of water vapor mixing ratio, temperature, wind speed and wind direction data measured by flux tower. The authors found synoptic-scale transport like the summer cold front in northern Wisconsin caused rapid change of CO_2 mixing ratio relative to what would be expected from biological processes. Similarly, many studies [*Bianchi et al.*, 2009; *Boutin et al.*, 2008; *Keppel-Aleks et al.*, 2012; *Lee et al.*, 2012; *Mahadevan and Archer*, 2000; *Parazoo et al.*, 2008; Pal et el., 2020] indicated that spatial CO_2 or XCO_2 variations are strongly related with synoptic-scale weather events, which are related to wind speed, wind direction, and potential temperature variations.

CO_2 frontal changes were observed by in-situ data in *Parazoo et al.* [2008], in which in-situ data were analyzed over synoptic time scales to observe the whole frontal passage in time. In the case of cold fronts, CO_2 changes as seen from in-situ continuous sites were found to have higher prefrontal CO_2 than postfrontal CO_2 at some sites like SGP (Southern Great Plains of North America, characterized by agriculture), WKT (Great Plains of North America in a region of strong moisture gradient, characterized by cattle grazing) and SBI (Sable Island, Island off the coast of Nova Scotia) in summer. *Parazoo et al.* [2008] used these observations together with models to decompose the components of the boundary layer CO_2 budget in the midlatitudes and found that the horizontal advection component is responsible for 60-70% of CO_2 daily variations on average in boundary layer, and thus dominates the variability seen in frontal gradients of CO_2.

Keppel-Aleks et al. [2012] found that the temporal variations in TCCON retrievals of XCO_2 at Park Falls, Wisconsin are primarily driven by non-local effects, i.e. transport of CO_2 from upstream, which is again a combination of regional scale fluxes and atmospheric motions. They also found that large-scale gradients of XCO_2 are highly correlated with synoptic-scale variations in free tropospheric potential temperature (θ).

Surface measurements like TCCON are made from fixed locations in space, and thus may miss signals from atmospheric CO_2 gradients such as fronts. Within the ACT-America (https://act-america.larc.nasa.gov) project, seven airborne campaigns across three regions in the eastern United States were conducted to study the transport and fluxes of atmospheric carbon dioxide and methane [*Pal et al.*, 2020] in which the seasonal variations of CO_2 concentration across frontal gradients (CO_2 concentration at warm sector minus that at cold sector) and fair weather conditions are apparent in the planetary boundary layer (PBL) in the mid-Atlantic, mid-west U.S., and south U.S. to Gulf of Mexico regions in summer 2016. *Pal et al.* [2020] illustrated that PBL CO_2 mixing ratio averaged in warm sectors was on average 15 ppm greater than in cold sectors in their 7 cases in summer.

In order to complement previous studies with TCCON, which observe gradients with respect to time, we examine OCO-2 XCO_2 differences in space across cold fronts as the satellite passes over the frontal boundary. CO_2 frontal differences observed by ACT-America flights are a reference against which to assess OCO-2 observations, with the caveat that magnitudes of spatial

gradients are not directly comparable given the different scales that the observations represent, i.e. the column average versus carbon dioxide concentration in or near the boundary layer, which is more responsive to convection and surface fluxes [*Keeling et al.*, 1976; *McClure et al.*, 2016; *Thoning et al.*, 1989].

There are two major questions in this work:

1. How does OCO-2 XCO_2 vary near frontal boundaries?
2. Are these variations across fronts distinct from climatological north-south gradients, when no front is present?

These two questions are aimed at the scales of atmospheric motion on which OCO-2 data varies, which is a necessary piece of knowledge for properly quantifying the representativeness of models assimilating OCO-2 retrievals. In a simulation study, *Corbin and Denning* [2006] found that coarse models did a poor job of representing the expected variability of OCO-2 data, resulting in large errors that would lead to biased flux estimates. The recommendation was that models with a spatial resolution of 1° by 1° in latitude and longitude are necessary to keep the representativeness errors less than 0.5ppm. We examine scales that are of this order.

3 Data and Methods

3.1 OCO-2 Retrievals of XCO_2

Launched in 2014 the National Aeronautics and Space Administration (NASA), OCO-2 flies in a sun-synchronous, near-polar orbit over a 16-day (233-revolution) repeat cycle and crosses the equator at about 1:30 PM Mean Local Time (MLT) (https://oco.jpl.nasa.gov/mission/quickfacts/). The OCO-2 spacecraft carries a single instrument that incorporates 3 high-resolution spectrometers collecting reflected sunlight, one in the molecular oxygen (O_2) A band, centered near 765 nm, and other two in the spectral bands near 1610 and 2060 nm. Collecting 24 spectra per second, OCO-2 yields about a million raw observations each day over the sunlit hemisphere. After screening is applied to filter out cloudy and overly polluted scenes, radiance measurements are used to infer XCO_2 with a "full-physics" retrieval algorithm [*O'Dell et al.*, 2018]. Clouds and optically thick aerosols preclude observations of the full atmospheric column in many regions, especially where there are weather phenomena like fronts, storms and snow. Retrievals of XCO_2 also fail when the solar zenith angle is too high, or when there are is low surface albedo such as in the case of snow and ice, which causes low Signal to Noise Ratio (SNR) (O'Dell et al. 2018). The fraction of soundings passing in the tropics is larger than at higher latitudes relative to sub-solar latitudes (>23°N in June and >23°S in December) and the passing rates are higher at bright than dark surfaces [*O'Dell et al.*, 2018], due to smaller solar zenith angles in tropics. The standard quality filter is applied to all converged retrievals to screen out scenes that are expected to be of poor quality due to these issues (O'Dell et al. 2018). Bad quality data are removed when analyzing XCO_2 differences across cold fronts in our study. With this approach, over 100,000 cloud-free full-column good quality XCO_2 observations are collected globally by OCO-2 each day.

In this study, we use XCO_2 from OCO-2 Version 9r Level 2 (L2) Lite product from 2015 to 2019, an example is given in Fig.1 on Aug 5th, 2016, in which we overlay various OCO-2 XCO_2 onto Aqua-MODIS RGB images from Worldview. Color in the OCO-2 track represents XCO_2 values. Version 9, released in October 2018, was the latest version of OCO-2 data before July 2020 when Version 10 was released, and had the lowest biases and highest throughput of any version so far [*Kiel et al.*, 2019]. Version 9 includes updated radiometric calibration for the

L1b product, updated spectroscopic parameters, the addition of a stratospheric aerosol type, and a more realistic treatment of surface reflectance, which were included in Version 8. Additionally, corrections have been made for differences in pointing between the 3 bands (Kiel et al, 2019) as well as a fix related to processing algorithm inputs. For large scale measurements, a previously reported positive bias with respect to models over southern hemisphere mid-latitude oceans is greatly reduced, though regionally coherent biases still remain at a significant level (~1 ppmv) [*O'Dell et al.*, 2018].

3.2 Detection of frontal boundary

3-hourly weather maps of surface analysis, mostly at 18UTC or 21UTC from Weather Prediction Center (WPC) in NOAA are used to locate days in which cold fronts were present somewhere in the Conterminous United States (CONUS) and Mexico between 20°N and 55°N . Only fronts with both warm and cold sectors all included in this domain are counted (i.e., cases in which part of warm or cold sectors locate over ocean or land out of the given domain are not included). Only summer cold fronts are considered because we find a sufficient number of OCO-2 observed cold front cases in summer between 2015 and 2019 for statistical analyses, while the other seasons have too few for this purpose. Further, since the growing season takes place in summer, we anticipate the behavior we observe will be related to general strong CO_2 uptake and net ecosystem exchange (NEE). *Pal et al.* [2020] has extensively analyzed the summertime frontal signatures as seen from ACT-America, and so this analysis can be compared more directly to published results.

Figure 2 shows an example of a cold front in Nebraska and Kansas at 18 UTC on August 5th, 2016 from NOAA surface analysis. Due to the fact that OCO-2 overpass times ranging from 15 UTC over the western Atlantic Ocean to 21 UTC over west coast of the U.S. each day, we choose the weather analysis at 18 UTC or 21 UTC, depending which is closest to the frontal overpass time. For visual analysis, we use the "OCO-2 MODIS Vistool" (https://github.com/hcronk/oco2_modis_vistool) developed by Heather Cronk from Colorado State University, which co-locates MODIS Aqua RGB images from Worldview using the NASA GIBS API with OCO-2 data fields. The tool has been used for case study analysis in support of OCO-2 cloud and aerosol screening validation (Taylor et al, 2016), as well as studies of local features in XCO_2 data (Bell et al, 2020). We employ the Vistool to visually identify and align the NOAA surface analysis with MODIS and OCO-2 imagery, enabling a visual determination of frontal crossing by the OCO-2 track.

Frontal zones, usually marked by sharp horizontal gradients in wind and temperature, are often observed with a cloud band and precipitation. Moisture varies sharply near the frontal boundary as seen from the strong gradients in dew point and equivalent temperature. The strong temperature gradient and moisture gradient across the front account for clouds over the frontal zone. XCO_2 retrievals either fail to converge or are screened in the presence of cumulus cloud related to the cold-frontal rainband at the leading edge [*Hobbs*, 1978] and thus XCO_2 at the frontal boundary is not available, implying that near frontal XCO_2 dynamics are hidden under clouds and not visible from space [*Corbin and Denning*, 2006]. We identify the band-like cloudy areas from the MODIS satellite image near the frontal boundary located in the surface analysis to be frontal zones, and the OCO-2 track north of the cloudy area.

Due to the filtering of OCO-2 XCO_2 data in cloudy areas, we define the first soundings nearest the cold and warm sector boundaries and then define the lengths of both warm and cold

sectors using the soundings within 3 degrees of latitude of these soundings for the purpose of calculating XCO2 differences across the frontal boundary. We performed a sensitivity study and determined that the length of the warm and cold sectors affects the absolute value of the differences, but not their significance (Figure 6).

A 3-sounding running mean is used to "smooth" the soundings in order to reduce the effects of outliers. We define the ΔXCO_2 frontal contrast as the difference between the warm sector mean XCO_2 the cold sector mean XCO_2, after this smoothing is applied. We apply the above method in the cases in summer (June, July, and August) for days in 2015 to 2019 during which there were a cold front and an instantaneous satellite track from OCO-2 over the CONUS and north Mexico (land between 20°N~55°N latitude, 50°W~140°W longitude).

3.3 Significance Test

We utilize a statistical method to explore the significance of the frontal contrasts over and above the day to day local variability of XCO_2 as well as the scatter of the OCO-2 data itself. There are stationary patterns in atmospheric CO_2 that arise from a climatological north-south gradient in surface fluxes as well as atmospheric flow patterns. As can be seen in Figure 5(a), which shows the monthly mean XCO_2 aggregated to 1° latitude and longitude boxes, there is a general depletion in northern XCO_2 relative to southern XCO_2. Solar-induced chlorophyll fluorescence (SIF) from OCO-2 and enhanced vegetation index (EVI) derived from MODIS suggest that photosynthesis of corn belt is stronger than less productive regions at lower latitudes, but at the same longitude in US, which could be a cause of this north-south gradient. Since this gradient could be mistaken for a frontal gradient if the timing and location is fortuitous, we construct a climatology of OCO-2 tracks passing through the study region on non-frontal days and determine the significance of the frontal differences over and above climatological differences in XCO_2. The method we use to construct the climatology is:

1. Randomly select an OCO-2 CONUS overpass when there is not a front if the length of that overpass is longer than [length of gap + 3 degrees of latitude (length of warm sector) + 3 degrees of latitude (length of cold sector)], and compute the XCO_2 differences with those lengths in the same manner as for the frontal days;
2. Repeat the random selection and computing for 1000 times in summer from 2015 to 2019.

The sample statistics of the climatology are used to determine whether XCO_2 contrasts across fronts are statistically different than non-frontal spatial contrasts in XCO_2. This analysis utilizes OCO-2 data, and so tests whether OCO-2 retrievals exhibit different synoptic scale variation on frontal days versus non-frontal days.

4 Results

4.1 XCO_2 differences across cold fronts and significance tests

Sample overpasses are displayed in Figure 4 for a cold front on Aug 5^{th,} 2016, where individual OCO-2 XCO_2 values are plotted versus latitude. The gap in the middle of the plot is the location of the cloud-covered region near the frontal boundary, which causes soundings to be screened out by prescreeners or filtered. This is reflected in the gradient of 2m dewpoint taken from MERRA-2. The warm sector has elevated mean XCO_2 (402.33 ppm) relative to the cold

sector mean (397.9 ppm), and their difference (4.426 ppm) is greater than the variability in each sector.

We found 66 summer cases from 2015 to 2019 in which a cold front was observed by OCO-2. In these five years, there are 12 frontal cases in 2015, 20 in 2016, 12 in 2017, 13 in 2018 and 11 in 2019. The contrast value is displayed in Figure 6 for all 66 cases. The error bar is defined to be the mean of the cold and warm side XCO_2 sample standard deviations. Figure 6 shows a general pattern of strong positive summertime frontal contrasts, with 39 of 66 cases having a frontal contrast of more than 1.026 ppm (the sum of the mean of climatology and its standard error).

Statistics for the different seasons are given Table 1. The average XCO_2 frontal contrasts for all five summers +0.981 ppmv (2015), +2.742 ppmv (2016), +1.125 ppmv (2017), +1.402 ppmv (2018), +1.861 ppmv (2019), and +1.762 ppmv for all summer cases. In spite of strong positive contrasts between warm and cold sectors on the majority of days, there are also individual days with negative changes across cold fronts such as Aug 28th, 2015 over Oklahoma and Jun 15th, 2017 over Iowa.

In addition to convergence of air in the vicinity of frontal boundaries, surface fluxes contribute to the size of the contrast. In the wintertime, much of the biosphere is inert, and hence CO_2 flux from plants is largely driven by spatially homogeneous respiration signals [*Raich and Schlesinger*, 1992; *Reichstein et al.*, 2005], while in the summer, CO_2 is depleted over productive regions in the boundary layer and, to a lesser extent, the total column. For example, growing regions such as the corn belt in the mid-western U.S. tend to have lower XCO_2 in the growing season than less productive regions such as shrublands and savannahs in south and central U.S., especially in north Mexico, New Mexico and south Colorado, as is depicted in Figure 5 for the gridded average of all OCO-2 soundings taken in summer of 2016. It is important to distinguish between these climatological differences in XCO_2 and frontally-induced differences in XCO_2.

As detailed in Section 3, we randomly selected 1000 non-frontal orbits in summer between 2015 and 2019 and calculate the assumed "frontal" differences in the same manner as for each of the true frontal boundary crossings. The climatological XCO_2 contrast is due to stationary atmospheric gradients in XCO_2, which are likely the result of flux differences between northern growing regions and southern grasslands [*Baker et al.*, 2010], coupled with upper level atmospheric flow features. Large-scale waves in higher latitudes do not tend to move southward because of the global wind patterns or the atmospheric circulation, resulting in weak meridional mixing of atmospheric CO_2 [*Wang et al.*, 2007]. As shown in Table 1, the mean of 1000 non-frontal XCO_2 differences is 1.074 and the standard error is 0.061. Our goal is to determine whether frontal contrast crossings are distinct from this climatological contrast obtained for fair weather cases.

Examining Table 1, we can compare the individual frontal crossings of OCO-2 with the climatology, which by construction contains the stationary seasonal differences discussed in the last paragraph. We find a number of individual days in each summer with differences that lie outside the 1σ confidence interval around the mean: 7 out of 12 in 2015, 17 out of 20 in 2016, 10 out of 11 in 2017, 8 out of 12 in 2018 and 8 out of 11 in 2019. Based on mean and standard deviation of both 66 XCO_2 frontal difference and 1000 assumed front cases, Student's T-test (with values shown in Figure 6) suggests that in the mean, frontal differences in OCO-2 XCO_2 are distinct from non-frontal north-to-south differences with the definition of 3° of latitude.

Sensitivity test results in Figure 7 reveals that, with shorter frontal sector definition, summer XCO_2 frontal differences in 2015-2019 remain significantly different from the climatology. T

scores from two-tailed Student's T-test and their corresponding p values in Figure 7 suggest that we can reject the null hypothesis (i.e., summer XCO_2 frontal differences are equal to non-frontal differences) at a 95% confidence level. P values of T scores for 3°, 2.5°, 2°, 1.5° latitude definitions are always less 0.05, indicating that our definition of cold and warm sector is not a key determinant of this finding.

In comparison with CO_2 frontal contrast in ACT-America campaign in *Davis et al.* [2018], we find similar patterns to Pal et al (2020): positive differences in summer, even though results from ACT-America campaign are measuring in situ CO2 concentration instead of XCO_2. This agreement is in spite of the fact that ACT America is sampling directly at the frontal boundary, rather than at larger scales like OCO-2. This seems to indicate that the larger scale forcing is driving the sign of the gradient across the frontal boundary, as opposed to surface processes near the frontal boundary that are affected by changes in radiation due to cloud cover or small scale atmospheric features.

4.2 The relationship between the strength of cold fronts and XCO_2 differences

Surface fronts are coincident with cyclones at upper levels, probably evolving from baroclinic waves, which tend to be strongest over the ocean, but can develop over land [*Wallace and Hobbs*, 2006]. The strength of the upper-level cyclone is associated with the scale and strength of surface fronts, which is also relative to surface temperature gradient, pressure gradient, wind speed and direction. Considering wind speed, temperature and specific humidity, *Parazoo et al.* [2008] illustrated that frontal CO_2 is related to deformational compression and strong advection along the front, which is also sensitive to locations and seasons. In order to explore the relationship between the strength of cold fronts and the magnitude of XCO_2 frontal difference, we examined the correlation between the XCO_2 frontal difference and temperature difference on each side of the front, with surface temperature under OCO-2 track. The resulting small squared correlation coefficient ($R^2 = 0.0053$) suggests that there is little evidence that XCO_2 frontal difference is related to frontal strength if temperature discontinuity considered only. However, this conclusion may be limited by cloudy area as seen from OCO-2. The gap distance also has weak correlation with XCO_2 frontal difference ($R^2 = 0.0441$), which is due to limited samples as well.

5 Discussion

OCO-2 data reveal that XCO_2 frontal crossings exhibit a consistent pattern: the mean XCO_2 on the warm side is generally greater than the cold side. These synoptic scale patterns in XCO_2 are distinct in magnitude from days when there are no fronts: summer differences are greater than the climatology would suggest from stationary atmospheric flow patterns. The climatology does suggest that the larger scale fluxes play an important role, as their mean difference across the assumed frontal gap is greater than 0. This means that the fronts themselves are enhancing these differences due to surface fluxes and climatological atmospheric transport.

Similarly to *Corbin and Denning* [2006], our results suggest that atmospheric chemistry transport models (ACTMs) attempting to reproduce OCO-2 data should resolve the synoptic spatiotemporal CO_2 gradients between airmasses at a minimum to avoid misrepresenting the data variations incorrectly. This is critical information, as some current global scale off-line ACTMs resolve transport only at the scales of several hundreds of kilometers (e.g. most of the models in the OCO-2 Model Intercomparison Project described by *Crowell et al.* [2019]). The impact of

this representation error on surface flux estimates is difficult to assess without further study of the models themselves, and is outside the scope of this observational study.

The results of our study would benefit from a larger set of cases, which would increase confidence. The number of cases are limited bythe sparse coverage of OCO-2 and the need for serendipitous timing of overpasses with fronts. Future missions such as the Geostationary Carbon Observatory (GeoCarb,*Moore III et al.* [2018]) will provide many opportunities to study the interaction between synoptic scale atmospheric motions and fluxes due to their much wider swath and daily revisits.

Future work is to distinguish between the roles of flux and transport for those seasonal variations of frontal differences. This analysis will require a well-calibrated atmospheric chemical transport model that resolves atmospheric motions at sufficiently high spatial resolution to reproduce the observed features in both the airborne measurements and the satellite data, which is currently in development. That work is the subject of a publication that is currently in preparation.

6 Conclusions

The preceding analyses demonstrated that across frontal boundaries OCO-2 XCO_2 retrievals observe differences that are distinct from the climatological XCO_2 north-south gradient present over the CONUS and north Mexico. OCO-2 XCO_2 differences across cold fronts were shown to exhibit similar qualitative behavior to that seen in previous literature, such as *Parazoo et al.* [2008]. The differences we found are naturally of a smaller magnitude than those found in the atmospheric boundary layer due to dilution of the lower tropospheric signal in the total column. These findings are also in agreement with aircraft observations made as part of the ACT-America campaign, which seems to imply that frontal dynamics drive non-local differences in CO_2, and hence models must be able to resolve these atmospheric features to properly make use of these data. Coarse models may misinterpret these transport-induced signals as local flux-induced, and thus lead to a biased flux estimate. These considerations are important for proper use of current and future spaceborne sensors like OCO-3, GOSAT, GOSAT-2, and GeoCarb [*Moore III et al.*, 2018], which will observe broader regions with a mapping-like approach at different times of day and thus, when used in conjunction with one another will lead to stronger inference on surface fluxes (and thus potentially a stronger bias in ill-equipped models).

Acknowledgement: QW and SC supported by NASA Grant Number 80NSSC18K0896. Co-author SP was supported by NASA Grant Number 80NSSC19K0730 and Texas Tech University start up research grant.

References

Baker, I., S. Denning, and R. Stöckli (2010), North American gross primary productivity: regional characterization and interannual variability, Tellus B: Chemical and Physical Meteorology, 62(5), 533-549.

Bianchi, A. A., D. R. Pino, H. G. I. Perlender, A. P. Osiroff, V. Segura, V. Lutz, M. L. Clara, C. F. Balestrini, and A. R. Piola (2009), Annual balance and seasonal variability of sea-air CO2 fluxes in the Patagonia Sea: Their relationship with fronts and chlorophyll distribution, Journal of Geophysical Research: Oceans, 114(C3).

Boutin, J., L. Merlivat, C. Hénocq, N. Martin, and J. Sallée (2008), Air-sea CO2 flux variability in frontal regions of the Southern Ocean from Carbon Interface Ocean Atmosphere drifters, Limnology and Oceanography, 53(5part2), 2062-2079.

Corbin, K. D., and A. S. Denning (2006), Using continuous data to estimate clear-sky errors in inversions of satellite CO2 measurements, Geophysical research letters, 33(12).

Crowell, S., D. Baker, A. Schuh, S. Basu, A. R. Jacobson, F. Chevallier, J. Liu, F. Deng, F. Liang, and K. McKain (2019), The 2015–2016 carbon cycle as seen from OCO-2 and the global in situ network, Atmospheric Chemistry and Physics, 19(15), 9797-9831.

Davis, K., S. Pal, T. Lauvaux, E. Browell, J. DiGangi, B. Gaudet, N. Miles, M. Obland, S. Richardson, and D. Stauffer (2018), Synoptic and Meso Scale Variability in Greenhouse Gases across Fronts in Four Seasons, paper presented at AGU Fall Meeting Abstracts.

Enting, I. G. (2002), Inverse problems in atmospheric constituent transport, Cambridge University Press.

Gurney, K. R., R. M. Law, A. S. Denning, P. J. Rayner, D. Baker, P. Bousquet, L. Bruhwiler, Y.-H. Chen, P. Ciais, and S. Fan (2002), Towards robust regional estimates of CO 2 sources and sinks using atmospheric transport models, Nature, 415(6872), 626.

Gurney, K. R., R. M. Law, A. S. Denning, P. J. Rayner, D. Baker, P. Bousquet, L. Bruhwiler, Y.-H. Chen, P. Ciais, and S. Fan (2003), TransCom 3 CO2 inversion intercomparison: 1. Annual mean control results and sensitivity to transport and prior flux information, Tellus B: Chemical and Physical Meteorology, 55(2), 555-579.

Hobbs, P. V. (1978), Organization and structure of clouds and precipitation on the mesoscale and microscale in cyclonic storms, Reviews of Geophysics, 16(4), 741-755.

Hurwitz, M. D., D. M. Ricciuto, P. S. Bakwin, K. J. Davis, W. Wang, C. Yi, and M. P. Butler (2004), Transport of carbon dioxide in the presence of storm systems over a northern Wisconsin forest, Journal of the atmospheric sciences, 61(5), 607-618.

Keeling, C. D., R. B. Bacastow, A. E. Bainbridge, C. A. Ekdahl Jr, P. R. Guenther, L. S. Waterman, and J. F. Chin (1976), Atmospheric carbon dioxide variations at Mauna Loa observatory, Hawaii, Tellus, 28(6), 538-551.

Keppel-Aleks, G., P. Wennberg, R. Washenfelder, D. Wunch, T. Schneider, G. Toon, R. J. Andres, J. Blavier, B. Connor, and K. Davis (2012), The imprint of surface fluxes and transport on variations in total column carbon dioxide, Biogeosciences, 9(3), 875-891.

Kiel, M., C. W. O'Dell, B. Fisher, A. Eldering, R. Nassar, C. G. MacDonald, and P. O. Wennberg (2019), How bias correction goes wrong: measurement of XCO2 affected by erroneous surface pressure estimates, Atmospheric Measurement Techniques, 12(4).

Law, R. M., E. A. Kowalczyk, and Y.-P. Wang (2006), Using atmospheric CO2 data to assess a simplified carbon-climate simulation for the 20th century, Tellus B: Chemical and Physical Meteorology, 58(5), 427-437.

Lee, T. R., S. F. De Wekker, A. E. Andrews, J. Kofler, and J. Williams (2012), Carbon dioxide variability during cold front passages and fair weather days at a forested mountaintop site, Atmospheric environment, 46, 405-416.

Mahadevan, A., and D. Archer (2000), Modeling the impact of fronts and mesoscale circulation on the nutrient supply and biogeochemistry of the upper ocean, Journal of Geophysical Research: Oceans, 105(C1), 1209-1225.

Masarie, K., W. Peters, A. Jacobson, and P. Tans (2014), ObsPack: a framework for the preparation, delivery, and attribution of atmospheric greenhouse gas measurements, Earth System Science Data, 6(2), 375-384.

Masarie, K., R. Langenfelds, C. Allison, T. Conway, E. Dlugokencky, R. Francey, P. Novelli, L. Steele, P. Tans, and B. Vaughn (2001), NOAA/CSIRO Flask Air Intercomparison Experiment: A strategy for directly assessing consistency among atmospheric measurements made by independent laboratories, Journal of Geophysical Research: Atmospheres, 106(D17), 20445-20464.

McClure, C. D., D. A. Jaffe, and H. Gao (2016), Carbon dioxide in the free troposphere and boundary layer at the Mt. bachelor observatory, Aerosol Air Qual. Res, 16, 717-728.

Moore III, B., S. M. Crowell, P. J. Rayner, J. Kumer, C. W. O'Dell, D. O'Brien, S. Utembe, I. Polonsky, D. Schimel, and J. Lemen (2018), The potential of the geostationary Carbon Cycle Observatory (GeoCarb) to provide multi-scale constraints on the carbon cycle in the Americas, Frontiers in Environmental Science, 6, 109.

O'Dell, C., A. Eldering, P. O. Wennberg, D. Crisp, M. R. Gunson, B. Fisher, C. Frankenberg, M. Kiel, H. Lindqvist, and L. Mandrake (2018), Improved Retrievals of Carbon Dioxide from the Orbiting Carbon Observatory-2 with the version 8 ACOS algorithm.

Pachauri, R. K., M. R. Allen, V. R. Barros, J. Broome, W. Cramer, R. Christ, J. A. Church, L. Clarke, Q. Dahe, and P. Dasgupta (2014), Climate change 2014: synthesis report. Contribution of Working Groups I, II and III to the fifth assessment report of the Intergovernmental Panel on Climate Change, IPCC.

Pal, S., K. J. Davis, T. Lauvaux, E. V. Browell, B. J. Gaudet, D. R. Stauffer, M. D. Obland, Y. Choi, J. P. DiGangi, and S. Feng (2020), Observations of Greenhouse Gas Changes Across Summer Frontal Boundaries in the Eastern United States, Journal of Geophysical Research: Atmospheres, 125(5), e2019JD030526.

Parazoo, N., A. Denning, S. Kawa, K. Corbin, R. Lokupitiya, and I. Baker (2008), Mechanisms for synoptic variations of atmospheric CO 2 in North America, South America and Europe, Atmospheric Chemistry and Physics, 8(23), 7239-7254.

Raich, J. W., and W. H. Schlesinger (1992), The global carbon dioxide flux in soil respiration and its relationship to vegetation and climate, Tellus B, 44(2), 81-99.

Reichstein, M., E. Falge, D. Baldocchi, D. Papale, M. Aubinet, P. Berbigier, C. Bernhofer, N. Buchmann, T. Gilmanov, and A. Granier (2005), On the separation of net ecosystem exchange into assimilation and ecosystem respiration: review and improved algorithm, Global change biology, 11(9), 1424-1439.

Stephens, B., M. Long, R. Keeling, E. Kort, C. Sweeney, E. Apel, E. Atlas, S. Beaton, J. Bent, and N. Blake (2017), The O2/N2 ratio and CO2 airborne Southern Ocean (ORCAS) study, Bulletin of the American Meteorological Society.

Thoning, K. W., P. P. Tans, and W. D. Komhyr (1989), Atmospheric carbon dioxide at Mauna Loa Observatory: 2. Analysis of the NOAA GMCC data, 1974–1985, Journal of Geophysical Research: Atmospheres, 94(D6), 8549-8565.

Wallace, J. M., and P. V. Hobbs (2006), Atmospheric science: an introductory survey, Elsevier.

Wang, J. W., A. S. Denning, L. Lu, I. T. Baker, K. D. Corbin, and K. J. Davis (2007), Observations and simulations of synoptic, regional, and local variations in atmospheric CO2, Journal of Geophysical Research: Atmospheres, 112(D4).

Wofsy, S. C. (2011), HIAPER Pole-to-Pole Observations (HIPPO): fine-grained, global-scale measurements of climatically important atmospheric gases and aerosols, Philosophical Transactions of the Royal Society A: Mathematical, Physical and Engineering Sciences, 369(1943), 2073-2086.

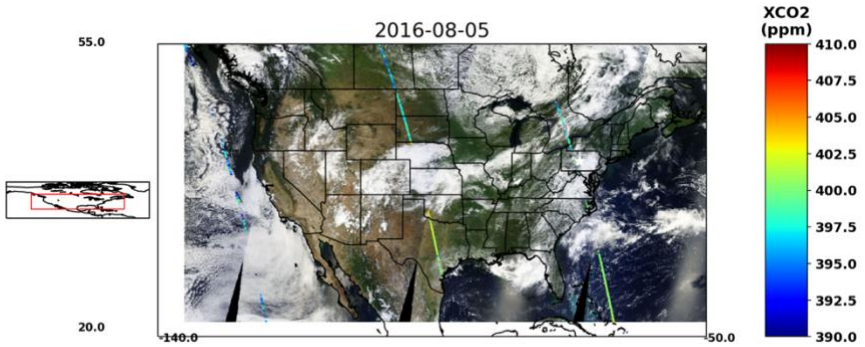

Figure 1 An example for OCO-2 tracks on August 5th, 2016. The satellite flies from east to west, south to north. The colors of the soundings vary with XCO_2.

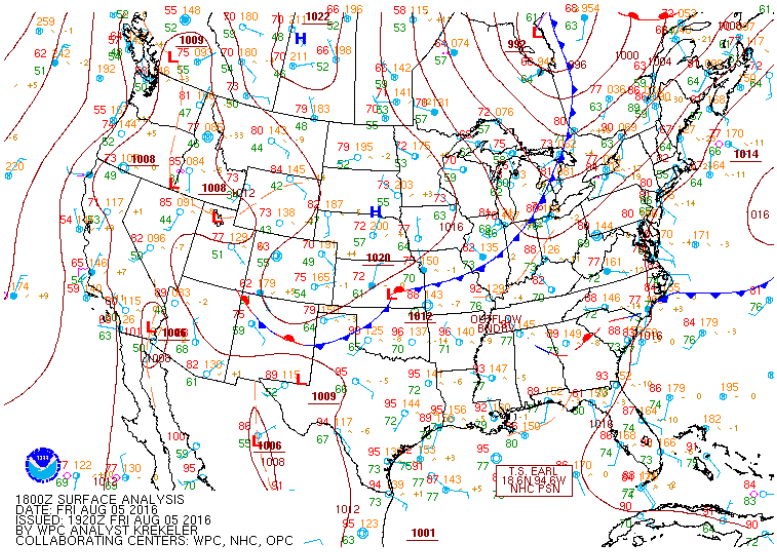

Figure 2 *An example for WPC surface analysis on August 5th, 2016, 18 UTC. This surface analysis is used to compare with OCO-2 tracks in Figure 3 to locate the cold front.* *(https://www.wpc.ncep.noaa.gov/archives/web_pages/sfc/sfc_archive_maps.php?arcdate=08/05/2016&selmap=2016080518&maptype=namussfc)*

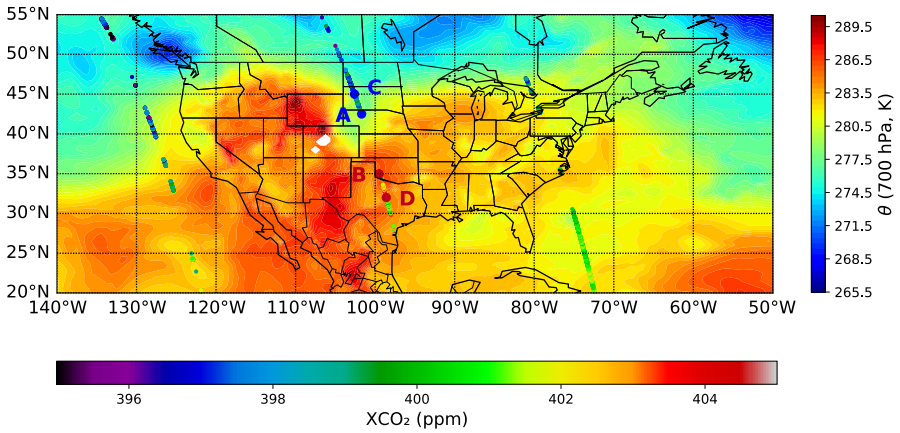

Figure 3 An example for OCO-2 tracks overlaid on the MERRA-2 potential temperature at 700 hPa on August 5th, 2016. The segment of track from A to C is used to calculate the cold sector mean XCO_2, while the segment from B to D is used to calculate the warm sector mean XCO_2. Distances between A and C, between B and D are both 3 degrees of latitude.

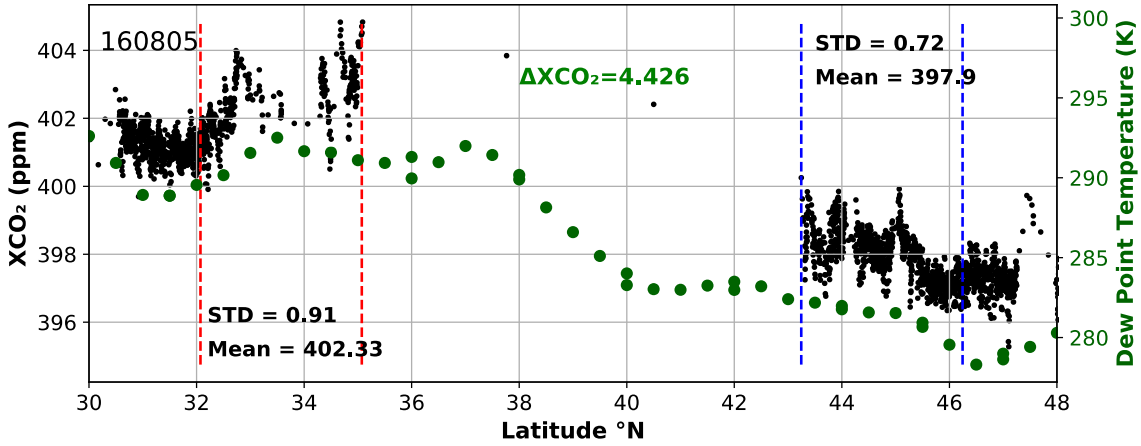

Figure 4 XCO_2 frontal gradient on August 5th, 2016. The left-hand section between red dashed lines is the warm sector in a cold front, black dots in this section are the satellite soundings in warm sector after a 3-sounding boxcar smoother is applied. Similarly, the cold sector is the region between the blue dashed lines on the right-hand side. The blank second section between the two sectors is missing data because of clouds. Green dots are dew point temperature at 2m above ground level. The gradients marked in the figures are the XCO_2 in warm sector minus that in cold sector.

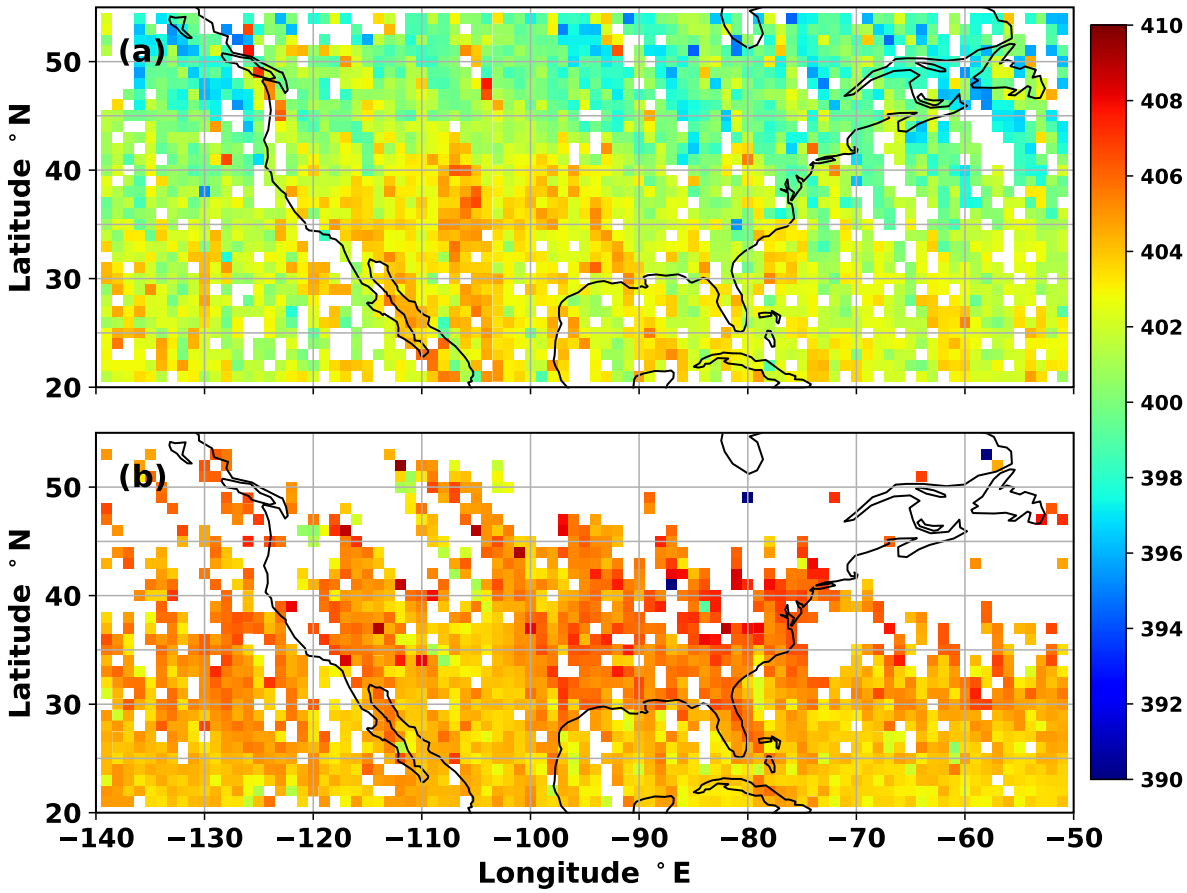

534

535 **Figure 5** Seasonal mean of OCO-2 XCO_2 (in 1° Latitude × 1° Longitude) over the CONUS
536 in 2016-2017 (a) in summer (JJA in 2016), (b) in winter (December in 2016, January and February
537 in 2017).
538

539

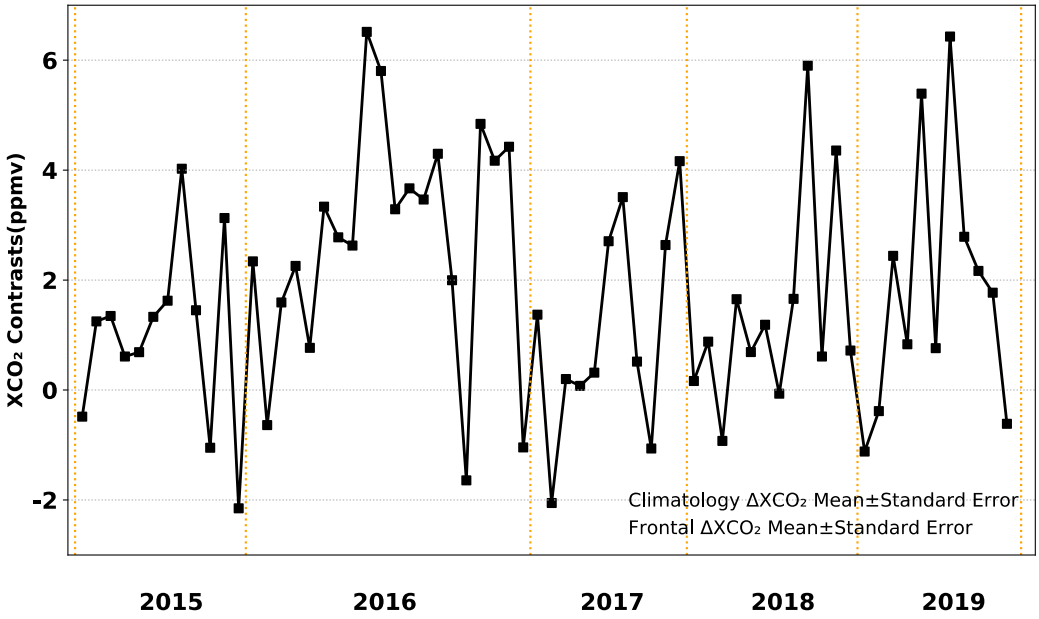

540

541 **Figure 6** 2015-2019 summer X_{CO_2} frontal differences (black dots) grouped by year.

542 Gray shade is climatological summer X_{CO_2} differences mean ±standard error and red shade is for
543 X_{CO_2} frontal differences mean ±standard error.

544

545

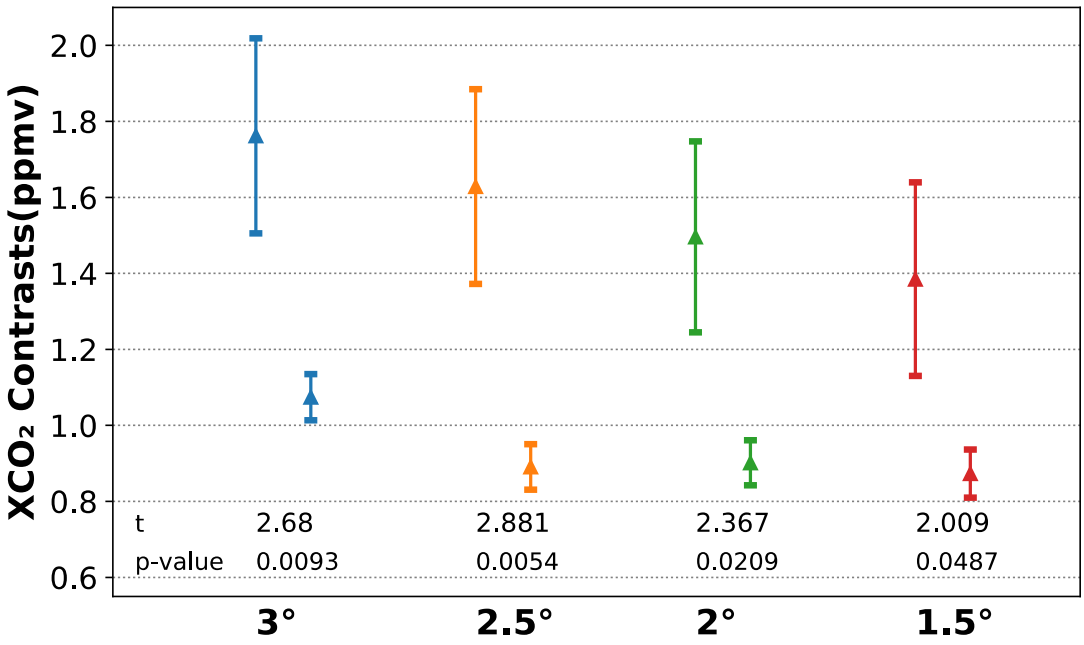

Figure 7 Error bar with mean and standard error of X_{CO_2} frontal differences and its assumed non-frontal differences. Left blue error bar is XCO_2 frontal differences defined 3° latitudes of both warm and cold sector, and right blue one is the error bar of 1000 assumed XCO_2 frontal differences; Orange, green, red left (right) error bars are similar to the blue left (right) one buf for 2.5°, 2°, 1.5° of latitudes.

564

565

	Frontal Cases						Non-frontal Cases
Year	2015	2016	2017	2018	2019	All	All
Counts	12	20	11	12	11	66	1000
Mean (ppmv)	0.981	2.742	1.125	1.402	1.861	1.762	1.074
Standard Error (ppmv)	0.465	0.470	0.558	0.528	0.686	0.257	0.061
25% Quantile (ppmv)	0.337	1.897	0.138	0.498	0.189	0.366	-0.128
Median (ppmv)	1.290	3.033	0.517	0.799	1.772	1.523	0.840
75% Quantile (ppmv)	1.496	4.203	2.672	1.653	2.615	3.248	2.209
Min (ppmv)	-2.151	-1.642	-2.056	-0.926	-1.119	-2.151	-6.281
Max (ppmv)	4.025	6.516	4.164	5.900	6.431	6.516	10.642

566 **Table 1** - Counts, mean and standard error, 25%quantile, median, 75%quantile, minimum and
567 maximum of $\mathbf{XCO_2}$ frontal contrasts for 2015-2019.
568
569
570
571
572
573
574
575
576
577
578
579
580
581
582

583